

Deploying Swarm Intelligence in Medical Imaging

Identifying metastasis, micro-calcifications and brain image segmentation

Mohammad Majid al-Rifaie*, Ahmed Aber[†], Duraiswamy Jude Hemanth[‡]

*Department of Computing, Goldsmiths, University of London
London SE14 6NW, United Kingdom
Email: m.majid@gold.ac.uk

[†]Department of Cardiovascular Sciences
University of Leicester Royal Infirmary
Leicester, LE2 7LX, United Kingdom
Email: aa721@le.ac.uk

[‡]Electronics and Communication Engineering Department
Karunya University, Coimbatore, India
Email: judehemanth@karunya.edu

This paper is a postprint of a paper submitted to and accepted for publication in IET Systems Biology journal and is subject to Institution of Engineering and Technology Copyright. The copy of record is available at IET Digital Library

ISSN 1751-8849

Received on 10th March 2015

Revised on 17th June 2015

Accepted on 23rd June 2015

doi: 10.1049/iet-syb.2015.0036

www.ietdl.org

Abstract—This paper proposes an umbrella deployment of swarm intelligence algorithm such as Stochastic Diffusion Search for medical imaging applications. After summarising the results of some previous work which shows how the algorithm assists in the identification of metastasis in bone scans and microcalcifications on mammographs, for the first time, the use of the algorithm in assessing the CT images of aorta is demonstrated along with its performance in detecting the nasogastric tube in chest X-ray. The swarm intelligence algorithm presented in this paper is adapted to address these particular tasks and its functionality is investigated by running the swarms on sample CT images and X-rays whose status have been determined by senior radiologists. Additionally, a hybrid swarm intelligence-Learning Vector Quantisation (LVQ) approach is proposed in the context of Magnetic Resonance (MR) brain image segmentation. The Particle Swarm Optimisation (PSO) is used to train the LVQ which eliminates the iteration-dependent nature of LVQ. The proposed methodology is used to detect the tumor regions in the abnormal MR brain images.

I. INTRODUCTION

Among the increasingly emergent fields in medicine is Computer Aided Diagnosis (CAD). Using the technique pre-

sented in this paper, radiologists are provided with a novel tool to examine the input images with greater confidence. Additionally doctors with different backgrounds and varying disciplines are able to use the tool with improved confidence. Medical students and junior doctors can utilise the provided tool to improve their ability in basic diagnostic skills. In this paper, a new CAD approach is developed using a swarm intelligence technique – Stochastic Diffusion Search (SDS) [1], [2] – which is generalised and adapted to be used in the context of four medical imaging modalities.

Understanding the basics behind the behaviour of the swarm intelligence algorithm and its connection to nature is vital. One of the important aspects in swarm intelligence is communication where information exchange plays a crucial role in the social interaction of social insects and animals. The swarm intelligence presented in this paper mimics the recruitment behaviour of a species of ants called *Leptothorax acervorum*.

Varying recruitment modalities are present in social animals and insects; they change from local to global, one to

many or one to one, and deterministic or stochastic. Depending on the particular social animals or insects in question and the environment, information exchange could take a simpler or a more complex form. What is shared among the entire set of information exchange strategies is the distribution of key information within the community of the swarm.

In this paper, which is an extended version of an earlier work (see [3]), initially, the swarm intelligence algorithm is introduced, followed by a brief summary to aortic aneurysm disease and the factors used to assess the disease and help plan an appropriate intervention. The swarms could provide the radiologist with extra assistance in identifying the anatomy in greater detail. Then, a brief explanation is also given on nasogastric (NG) tube and its use to provide an effective mechanism through which short-term nutrition can be given to critically ill patients.

One of the serious complications of NG tube placement is caused by inadvertent malpositioning. This can lead to severe harm or death if the patient is fed through it. This could possibly be prevented by deploying the swarm intelligence technique, providing extra information about the location of the tip of the tube, avoiding fatal human error.

After presenting the above-mentioned areas of interest, a detailed introduction is given on Stochastic Diffusion Search (SDS) algorithm which is adapted in order to be deployed in the context of the presented problems. The results are then detailed for each of the areas stated earlier and an exemplar analysis is given illustrating the behaviour of the method presented.

While the paper aims to demonstrate a novel way of addressing some of the presented medical imaging scenarios, the authors keep themselves away from the claim that the presented algorithm is an optimal solution to all medical imaging problems.

A. Previous Work and Summary of Current Research

In the initial work [4], the goal was to visualise the swarms behaviour when presented with a two dimensional canvas (e.g. bone scan). This work was well received as a potential educational tool for doctors in training and medical students. This led to the extension of the research in [5], [6] where the application of this swarm intelligence technique on bone scan was introduced in further details in different venues for researchers with medical and computer backgrounds. Later in [7], the statistical and mathematical models were presented for bone scans, and the application of the technique was extended to mammography.

In this work, we attempt to present a unifying and generalised framework of the potential of the algorithm, showing its capability in addressing various issues related to different scans and task; after summarising the results of our previous work, two novel applications of the algorithm are introduced:

- The first one is a two-phase process in which initially the swarms identify the location of the aorta within the CT scan. The swarms then set off to detect and highlight any possible calcifications around the aorta with the goal of assisting the radiologists to determine the extent of the calcification. This information can

help determine the best possible management of the disease. This task is particularly distinctive from the previous work, as a novel way of guiding the behaviour of the swarms is introduced, increasing their flexibility and functionality.

- The second application introduced in this work is the identification of the tip of the Nasogastric tube in chest X-rays. The significance of the accurate localisation of the tip of the tube is explained with details in this work.

In addition to the above, a hybrid swarm intelligence-Learning Vector Quantisation (LVQ) approach is proposed in the context of Magnetic Resonance (MR) brain image segmentation. The Particle Swarm Optimisation (PSO) is used to train the LVQ which eliminates the iteration-dependent nature of LVQ. The proposed methodology is used to detect the tumor regions in the abnormal MR brain images.

While an emphasis is given to the fact that this research does not aim to replace the expertise of the radiologists, all of the above-mentioned four applications provide the clinicians with a valuable adjunct to aid with the diagnosis as well as the management of patient. This method of interpreting images can also be used as an educational tool for doctors in training and medical students.

II. STOCHASTIC DIFFUSION SEARCH

This section introduces Stochastic Diffusion Search (SDS) [1], [2] – a swarm intelligence algorithm – whose performance is based on simple interaction of agents.

The SDS algorithm commences a search or optimisation by initialising its population and then iterating through two phases (see Algorithm 1)

Algorithm 1 SDS Algorithm

```

01: Initialising agents()
02: While (stopping condition is not met)
03:   Testing hypotheses()
04:   Determining agents' activities (active/inactive)
05:   Diffusing hypotheses()
06:   Exchanging of information
07: End While

```

In the test phase, SDS checks whether the agent hypothesis is successful or not by performing a hypothesis evaluation which returns a boolean value. Later in the iteration, contingent on the precise recruitment strategy employed (in the diffusion phase), successful hypotheses diffuse across the population and in this way information on potentially good solutions spreads throughout the entire population of agents. In other words, each agent recruits another agent for interaction and potential communication of hypothesis. This algorithm has been used alongside other swarm intelligence algorithms in several research topics including numerical optimisation and clustering. In standard SDS (which is used in this paper), *passive recruitment* mode is employed. In this mode, if the agent is inactive, a second agent is randomly selected for diffusion; if the second agent is active, its hypothesis is communicated (*diffused*) to the inactive one. Otherwise there is no flow of information between agents; instead a completely

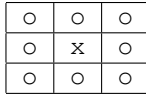


Fig. 1. Agent’s neighbours in test phase. The symbol \times represents the position of the agent and the \circ ’s represent the neighbours used during the test phase. As shown in the figure, the radius of the test is set to 1.

new hypothesis is generated for the first inactive agent at random (see Algorithm 2). Therefore, recruitment is not the responsibility of the active agents. In this work, activity of each agent is determined when its fitness is compared against a random agent (which is different from the selecting one); if the selecting agent has a better fitness (smaller value in minimisation problems) than the randomly selected agent, it will be flagged as active, otherwise inactive. Higher rate of inactivity boosts exploration, whereas a lower rate biases the performance towards exploitation.

Algorithm 2 Passive Recruitment Mode

```

01: For ag = 1 to No_of_agents
02:   If ( !ag.activity() )
03:     r_ag = pick a random agent()
04:     If ( r_ag.activity() )
05:       ag.setHypothesis( r_ag.getHypothesis() )
06:     Else
07:       ag.setHypothesis( randomHypothesis() )
08:     End If/Else
09:   End If
10: End For

```

A. Algorithm Procedure

SDS is a population based stochastic algorithm, adapted here to search for areas of metastasis or calcifications in the feasible solution space. The hypothesis vectors of the population are defined as follows:

$$x_i^g = [x_{i,1}^g, \dots, x_{i,D}^g], i = 1, 2, \dots, NP \quad (1)$$

where g is the current iteration, D is the dimension of the problem space ($D = 2$) and NP is the population size. In the first generation, (when $g = 0$), the i^{th} vector’s j^{th} component could be initialised as:

$$x_{i,j}^0 = x_{min,j} + r(x_{max,j} - x_{min,j}) \quad (2)$$

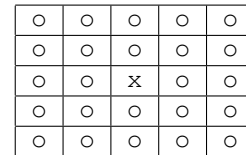
where r is a random number drawn from a uniform distribution on the unit interval $U(0, 1)$, and x_{min} , x_{max} are the lower and upper bounds of the j^{th} dimension, respectively. The initial status of all agents are set to false. In other words, each agent randomly picks a pixel from the image of the scan.

During the test phase of SDS algorithm, each agent’s status should be determined. The method used here to set the activity of the agents is to find the average of the colour intensity¹ ($avgIn$) of each agent and its neighbours (see Fig. 1). If $avgIn$ is within a specific range (problem dependent), the agent is flagged active, otherwise inactive.

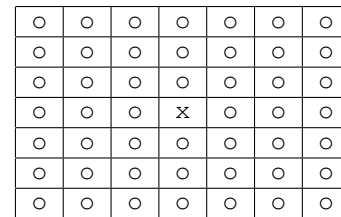
During the diffusion phase, each inactive agent randomly selects another agent from the population; if the selected agent is active, the selecting agent adopts the hypothesis (i.e. location) of the active agent and the information sharing takes place. The strategy used for information sharing is to randomly pick an area surrounding the active agent (see Fig. 2). Active agents also check their position by continuously picking a random pixel in the neighbourhood; this way, an area which does not have a good enough potential is discarded from one iteration (i.e. cycle of test and diffusion phases) to the next.

List of adjustable parameters for each experiments:

- Population size (S)
- Agent’s activity which is determined using the value of average intensity $avgIn$ (e.g. if $avgIn > \alpha$ the agent is set active, otherwise inactive). The value of α is also problem-dependent and it could be adjusted to increase or decrease the sensitivity of the system.
- Diffusion radius ($dRad$)
- Number of iterations (Itr)



(a)



(b)

Fig. 2. Diffusion area for (a) bone scans, mammographs and NG-tube; (b) AAA. The symbol \times represents the position of the active agent and the \circ ’s represent the accessible places during the diffusion phase. The reason behind the larger area considered for (b) is the greater radius of the area of interest in AAA (see Fig. 11).

III. X-RAY AND CT SCANS

This section provides an introduction to aortic aneurysm disease and nasogastric tube. For information about bone scan metastatic disease, mammography refer to [3].

A. Aortic Aneurysm Disease

The aorta is the main artery that carries the blood away from the heart to rest of the body giving rising to various branches for this purpose. Aortic aneurysm (AA) is a disease commonly found in patients above the age of 65. It is defined as a permanent localized dilation of the aorta that has at least a 50% increase in diameter as compared with the expected normal diameter of the aorta, which may vary according to age, sex, and body size [8].

¹ Colour intensity (In) signifies the brightness of pixels, $0 \leq In \leq 255$.

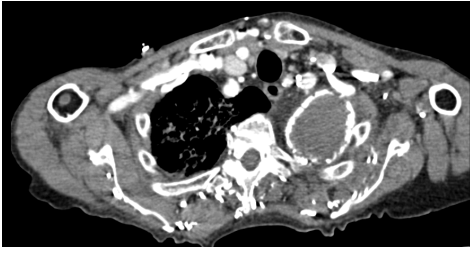


Fig. 3. A slide of CT scan showing aortic aneurysm disease

Each year approximately 15,000 people in the United States die from a ruptured abdominal aneurysm, rendering it the 15th leading cause of death in this country [9]. Thirty percent to 75% of patients with a ruptured Abdominal Aortic Aneurysm (AAA) die before they ever reach a hospital [10]. Even with surgery, an average 48% (95% CI 46% to 50%) perioperative mortality rate is associated with a ruptured AAA repair [11]. The overall mortality rate in patients with ruptured AAA ranges from 67% to 89% [10]. Therefore, detection of AAAs before rupture and elective repair can prolong survival and decrease the periprocedural complication rate.

The primary goal in Aortic Aneurysm treatment is to prolong survival through the prevention of rupture. The treatment options include the following [8]:

- Open surgical repair
- Endovascular repair (EVAR)
- Continued surveillance

Endovascular aortic aneurysm repair (EVAR) is considered a safer alternative to open surgery in selected patients. Its feasibility depends mainly on anatomic factors that represent the important predictors of success. Poor anatomic patient selection is generally associated with a higher risk for procedural complications and compromised long-term outcomes. Therefore pretreatment imaging is crucial for evaluating patient suitability for EVAR as well as appropriate planning to avoid complications mainly endoleaks. Computed tomographic angiography represents the current standard imaging used to evaluate the anatomy of aorta because it provides all the details needed for selection of patients who are suitable for EVAR.

Exclusion of the aneurysm sac is the main goal of EVAR, and clinical success is defined by the “total exclusion” of the aneurysm. However, at times, failure of the stent-graft to totally exclude blood flow to the aneurysm sac may occur. As a matter of fact, endoleak is the major cause of complications, and thus failure EVAR. When an endoleak occurs, it causes continued pressurisation of the aneurysm sac and may leave the patient at risk of an AAA rupture.

1) *Proximal neck of the aneurysm*: The pre-EVAR anatomical evaluation assesses several aspects of the anatomy of the aortic aneurysm including the proximal neck of aneurysm anatomy which is the most important predictor factor for a successful EVAR. The proximal neck is the segment of aorta above the aneurysm sac. An unfavourable neck anatomy, based on its diameter, length, angulation, morphology, and presence of calcification and mural thrombus, is the most frequent cause of exclusion from EVAR [12].

a) *Length*: To achieve a good seal and decrease proximal migration and type I endoleak rates, a length of at least 15-mm for infrarenal stent-graft fixation or 10-mm for transrenal stent-graft fixation, with barbs, hooks, or uncovered suprarenal stents, is recommended [13]. Patients who have a neck shorter than to 10-mm are unsuitable for EVAR

b) *Angulation*: A severe neck angulation ($> 60^\circ$) seems to be associated with a potentially higher risk of adverse events, especially type I endoleaks, as reported by studies [14], [15].

c) *Morphology*: The morphology of the proximal neck can be defined as straight (unchanged diameters), tapered (proximal diameter superior to distal), or reverse tapered (distal diameter superior to proximal by >3 -mm). A reverse tapered neck and a neck bulge are associated with a higher proximal endoleak rate and thus are contraindications for EVAR [16].

d) *Presence of calcification*: Calcification and mural thrombus are expressed in degrees of circumference. Mural thrombus and severe and extensive calcifications that cover more than 90 of the circumference of the aortic diameter in the proximal neck are associated with a higher risk for type I endoleak and stent-graft migration, respectively [13].

Assessing the anatomy of the aortic aneurysm for appropriate intervention is a difficult task and the use of the SDS algorithm helps segment the images and quantify some of the problems such as the calcification at different levels of the aorta. In this paper by assessing the level of calcifications at different parts of the proximal neck aneurysm aorta, the SDS can help identify suitable candidate for endovascular repair and potentially reduce the level of complications associated with mounting the endovascular graft in an unfavourable location.

B. Nasogastric Tube

Nasogastric tubes (tube inserted through the nose to the stomach) are commonly used for short-term nutrition in critically ill patients. Complications of nasogastric tubes frequently include inadvertent malpositioning and aspiration pneumonia that may cause severe harm or death. The National Patient Safety Agency (NPSA) in the United Kingdom received reports of 21 deaths and 79 cases of harm due to feeding into the lungs though misplaced NG tubes between September 2005-March 2011 [17]. The main cause of the harm in the investigated cases was the misinterpretation of the X-rays that were done to assess the position of the NG tube (see Fig. 4). X-ray assessment is usually done if the aspirate from the NG tube does not reflect the natural level of acidity of the stomach fluid content which is normally between 1-5.5 pH. It is vital to note that X-rays are used more commonly as obtaining an aspirate can be difficult in most of patients. The NPSA guidelines states that when assessing the NG position the following criteria should be strictly followed:

- The tube path follow the oesophagus/avoid the contours of the bronchi
- Assess that the tube does not bisect the carina or the bronchi (Airways)
- NG tube should cross the diaphragm in the midline



Fig. 4. Chest X-ray showing a misplaced Nasogastric tube

- The tip should be visible below the left hemidiaphragm

The careful interpretation of an X-ray to assess the position of an NG tube needs a trained eye. This might not be available at all times. This limitation in resources may lead to either misinterpretation by a junior doctor leading to a serious clinical incident or if there is a delay in the interpretation this can translate itself to a delay in feeding the patient for several hours. The SDS can help provide a tool to avoid the above scenarios by detecting the tip of the NG tube.

IV. APPLYING STOCHASTIC DIFFUSION SEARCH

In this paper, we are presenting a unique approach by deploying SDS to use in assessing medical images. This approach demonstrates a promising ability to undertake this task with similar level of sensitivity. Each scan used in this paper is processed by the SDS agents which are responsible for locating the desired areas.

The reproducibility and the accuracy of the SDS algorithm can be utilised in developing a standardised system to help interpreting medical images and prevent operator errors and discrepancies. This type of technologies can be employed as an adjunct to help radiologists assess the various types of images making the diagnosis more thorough and less time consuming. Additionally this technique can be effectively used to develop programs for teaching and training medical students and junior doctors.

A. Bone Scans

This section presents the results focusing on bone scans; however the methods used are extendible to other scans referred to in this work.

Below are the adjustable parameters that are determined depending on the problem in hand (i.e. identifying metastasis

in bone scan) and the machine used to generate the scans. In this experiment, they are defined as:

- $S = 10,000$
- $\alpha = 180$.
- $dRad = 2$
- $Itr = 10$

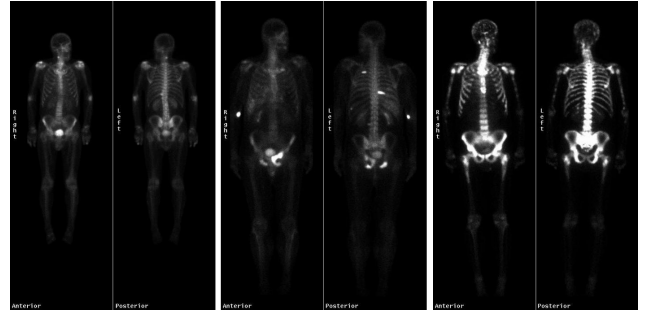


Fig. 5. Bone Scans. Typically 2–6 hours after intravenous administration of technetium-99m-labeled diphosphonates; brighter areas indicate a higher radiotracer uptake. As assessed by senior radiologists, left: Healthy; middle: partially affected; right: metastatic disease spread.

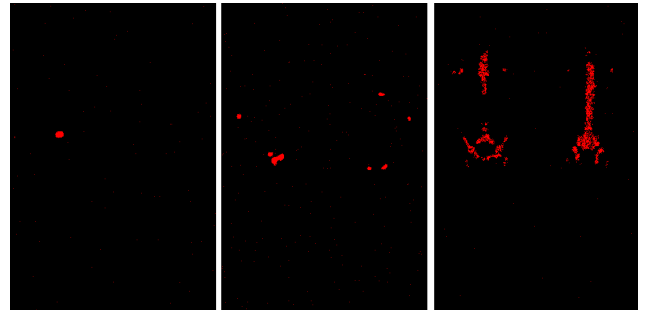


Fig. 6. The bone scans are processed using Stochastic Diffusion Search algorithm. Left: Healthy; middle: partially affected; right: metastatic disease spread.

As shown in Fig. 5, areas with higher potential of metastasis are identified. In bone scans, other than urinary bladder activity, faint renal activity, and minimal soft-tissue activity which are normally present in the scan (Fig. 5 Bottom-left), the existence of multiple, randomly distributed areas of increased uptake of varying size, shape, and intensity are highly suggestive of bone metastases (Fig. 5 Bottom-middle). Additionally as stated before, when the metastatic process is distributed, almost all of the radiotracer congregates in the skeleton, with little or no activity in the soft tissues or urinary tract (see Fig. 5 Bottom-right).

As shown in Fig. 5 and 9, areas with higher potential of metastasis and calcifications are identified. In bone scans, other than urinary bladder activity, faint renal activity, and minimal soft-tissue activity which are normally present in the scan (Fig. 5 Bottom-left), the existence of multiple, randomly distributed areas of increased uptake of varying size, shape, and intensity are highly suggestive of bone metastases (Fig. 5 Bottom-middle). Additionally as stated before, when the metastatic process is distributed, almost all of the radiotracer

congregates in the skeleton, with little or no activity in the soft tissues or urinary tract (see Fig. 5 Bottom-right).

In order to visually present the technique used, Fig. 7 illustrates how agents congregate over the areas of interest over time (i.e. iterations) when fed with the scans as inputs of the algorithm. As the figure shows, successful agents diffuse their positions across the population and this way, information on potentially good solutions spreads throughout the entire population of agents. This process is caused through the recruitment strategy, where each agent recruits another agent for interaction and potential communication of the promising areas. Next, two models are presented to distinctively differentiate between different types of bone scans (e.g. not affected, affected and highly affected).

1) *Statistical Model:* Here, a statistical analysis, TukeyHSD Test [18], is performed to highlight whether there is a significant difference between the activity of the agents when processing the bone scans. Table I (a) shows the activity rate of the populations over each iteration. Three different samples are used for this analysis: Samples 1, 2 and 3 refer to the scans in Fig. 5 (left to right). Table I (b) shows that other than the first iteration where the agents are just initialised, different bone scans would result in significantly different activity rates. This could be used as an indicator, highlighting the difference between various scans and whether they are healthy, partially affected or the metastasis is spread.

TABLE I. ACTIVITY STATUS OF AGENTS PROCESSING BONE SCANS

(a) Mean \pm standard deviation of the number of active agents in each iteration is shown (rounded to the nearest number).

Itr	Sample 1	Sample 2	Sample 3
0	0 \pm 0	0 \pm 0	0 \pm 0
1	5 \pm 2	17 \pm 4	277 \pm 16
2	15 \pm 4	47 \pm 9	763 \pm 37
3	33 \pm 8	100 \pm 18	1602 \pm 76
4	66 \pm 18	201 \pm 31	2991 \pm 137
5	129 \pm 33	379 \pm 51	4992 \pm 188
6	245 \pm 62	697 \pm 84	7260 \pm 198
7	461 \pm 110	1250 \pm 141	8947 \pm 123
8	852 \pm 201	2201 \pm 230	9583 \pm 51
9	1557 \pm 351	3650 \pm 330	9708 \pm 22

(b) Based on TukeyHSD Test, if the difference between each pair of samples is significant, the pairs are marked (o - X shows that the right sample has significantly more active agents than the left one). This test uses 95% family-wise confidence level.

The aim is to show that agents dealing with scans which have different levels of metastasis exhibit significantly different behaviour.

Itr	s1 - s2	s1 - s3	s2 - s3
0	-	-	-
1	o - X	o - X	o - X
2	o - X	o - X	o - X
3	o - X	o - X	o - X
4	o - X	o - X	o - X
5	o - X	o - X	o - X
6	o - X	o - X	o - X
7	o - X	o - X	o - X
8	o - X	o - X	o - X
9	o - X	o - X	o - X

2) *Mathematical Model:* Visualising the data produced in Table I (a) could introduce another method of determining which of the three broad category (healthy, partially affected or the metastasis is spread) the bone scan falls into (see Fig. 8). This model is proposed here to calculate the first and the second derivatives using the following formulas:

$$f'_i{}^s = \sigma_i^s - \sigma_{i-1}^s \quad (3)$$

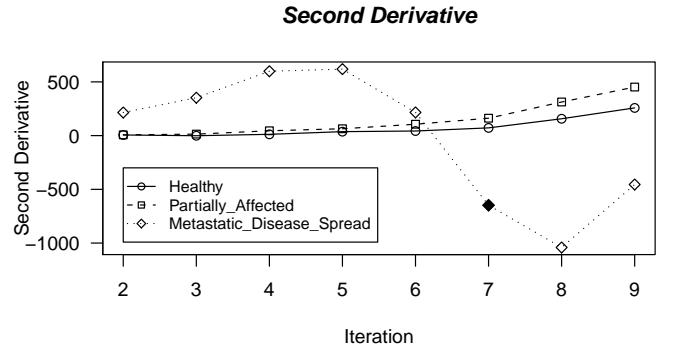
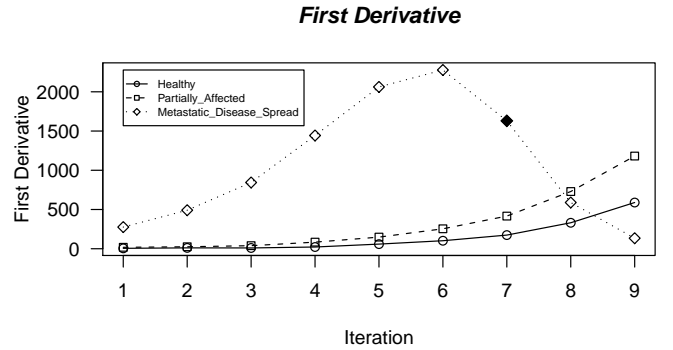
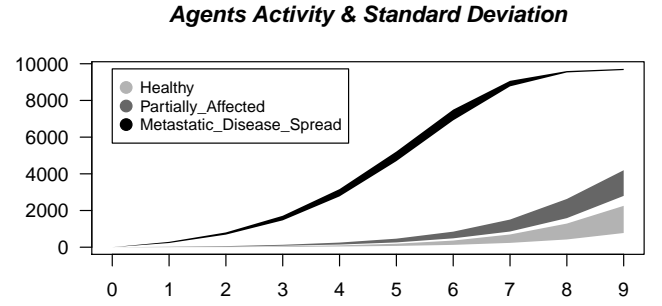
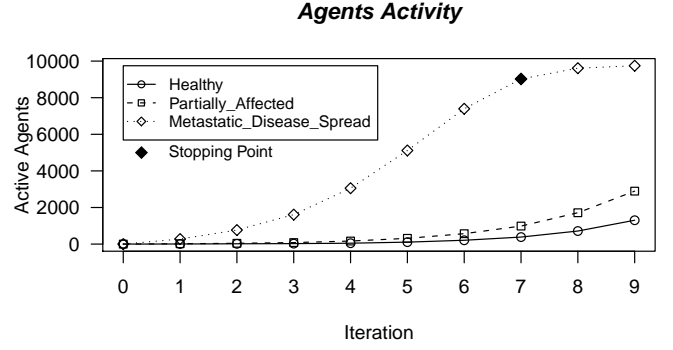


Fig. 8. Agents activity. The plots in this figure illustrate the activity of agents, the standard deviation, first and second derivatives on each iteration in the three sample bone scans. The 'stopping point' in the top plot shows the iteration number when SDS algorithm could terminate. This occurs when the value of the second derivative is negative (see Eq. 4).

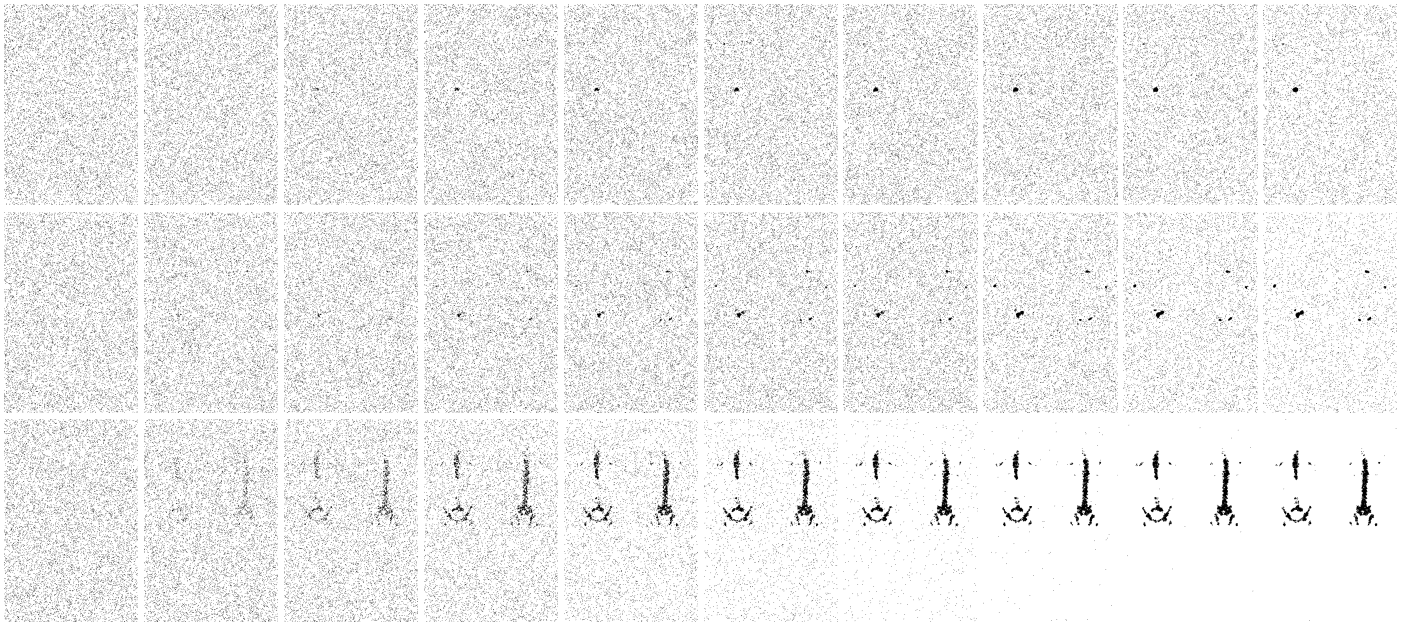


Fig. 7. SDS algorithm processing the bone scans in 10 iterations. Each row shows the behaviour of the agents when presented with one scan. Each scan is processed by 10,000 agents (illustrated as black dots) and through communication, agents explore different areas of the scans to identify potential areas of metastasis. The leftmost figures in each row show the location of the agents on the first iteration (given agents are initialised and randomly distributed in the search space, they are manifested as small black dots at this stage), and the rightmost ones represent the last iteration.

$$f''_i^s = \sigma_i^s - 2 \times \sigma_{i-1}^s + \sigma_{i-2}^s \quad (4)$$

where f' and f'' are the first and the second derivatives of function f respectively, σ represents the number of active agents, i is the iteration number and s is the bone scan sample number, $s = \{1, 2, 3\}$. The value of the second derivative (f'') can be used as an indicator to stop the algorithm. The rationale behind stopping the algorithm is that the activity of the agents has reached a point that allowing further process, would blur the congregation of the agents around less popular clusters. This is caused by the diffusion mechanism of the algorithm where there is higher probability of an inactive agents picking another one from within the larger clusters than the smaller ones.

Having discussed the functions of statistical and mathematical methods, the following three sections extends the use of SDS to mammographs, AAA's CT scans and NG-tube's X-ray.

B. Mammographs

One of the main aims of the CAD systems is to identify microcalcifications to help the radiologists make the diagnosis. Microcalcifications are sometimes difficult for the human film reader to detect because of their small size and low contrast, particularly if they are superimposed on dense glandular tissue. However, of all the signs of abnormality found on mammograms, microcalcifications are the easiest to detect automatically. Unlike small ill-defined masses, which may superficially resemble normal glandular tissue, microcalcifications have properties namely their very small size and high attenuation which differ significantly from those of normal background structures.

Adjustable parameters:

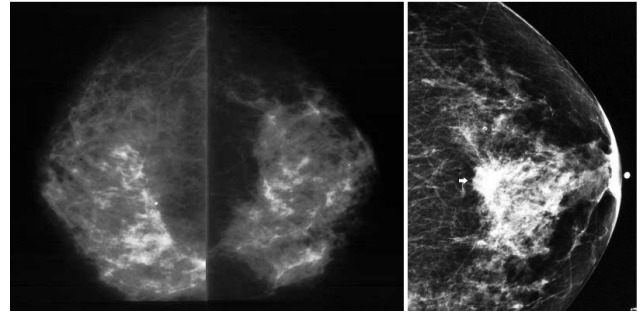


Fig. 9. Mammographs.

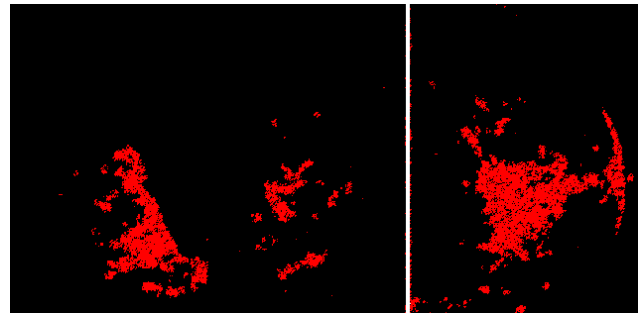


Fig. 10. Mammographs. Area with potential microcalcification particles are detected using the Stochastic Diffusion Search algorithm.

- $S = 10,000$
- $\alpha = 120$. As discussed earlier, this experiment requires a higher level of sensitivity and thus the threshold of α is set lower than the previous experiment.
- $dRad = 2$

- $Itr = 10$

Since smaller clusters are of interest in bone scan and specially mammographs, a different mechanism for determining the ‘stopping point’ is proposed. In this method, when $f'' < 0$ the algorithm reaches the stopping point. Fig. 9 shows that areas with higher potential of calcifications.

C. Aortic Aneurysm Disease

The SDS algorithm is utilised in this experiment to assess the proximal neck of the aneurysm and detect the level of calcification above the sac.

The agents are initialised throughout the search space (i.e. the CT image) in a two-phase mission, the first of which is to identify the location of the aorta within the scan, and the second phase highlights the existing calcification within the marked area. The adjustable parameters are empirically chosen as follows in each phase.

Phase one:

- $S = 1,000$
- $\alpha = 100$
- $\beta = 140$
- $dRad = 3$
- $Itr = 50$

Phase Two:

- $S = 1,000$
- $\alpha = 150$
- $\beta = 255$
- $dRad = 1$
- $Itr = 100$

In the first phase, since the radius of the area of interest is in one particular area (i.e. aorta, which exists in only one place in each scan), the diffusion phase is set to explore a bigger region of the search space around the active agent and thus the diffusion radius, $dRad$ is set to 3 units (see Fig. 2). This leads to the identification of the centre of aorta which is presented in Fig. 11 top.

Fig. 11 middle highlights the region where potential calcifications could be spotted by the swarms (within the bigger circle in the figure); once this region is located, the second phase commences where swarms congregate over the area of interest based on the value of $\alpha < avgIn < \beta$, which dictates the activity of the swarm and thus the convergence behaviour as shown in Fig. 11-bottom. As indicated above, in the second phase, the algorithm is allowed a smaller diffusion radius, $dRad$, but a larger number of iterations in order to ensure a total convergence of the swarms to more precise areas with the required colour intensity.

Once the swarms converge, the suitability of the scan is evaluated by measuring the activity rate of the swarms; this activity is directly related to the level of calcification in the aortic wall in that particular segment of the aorta. This helps

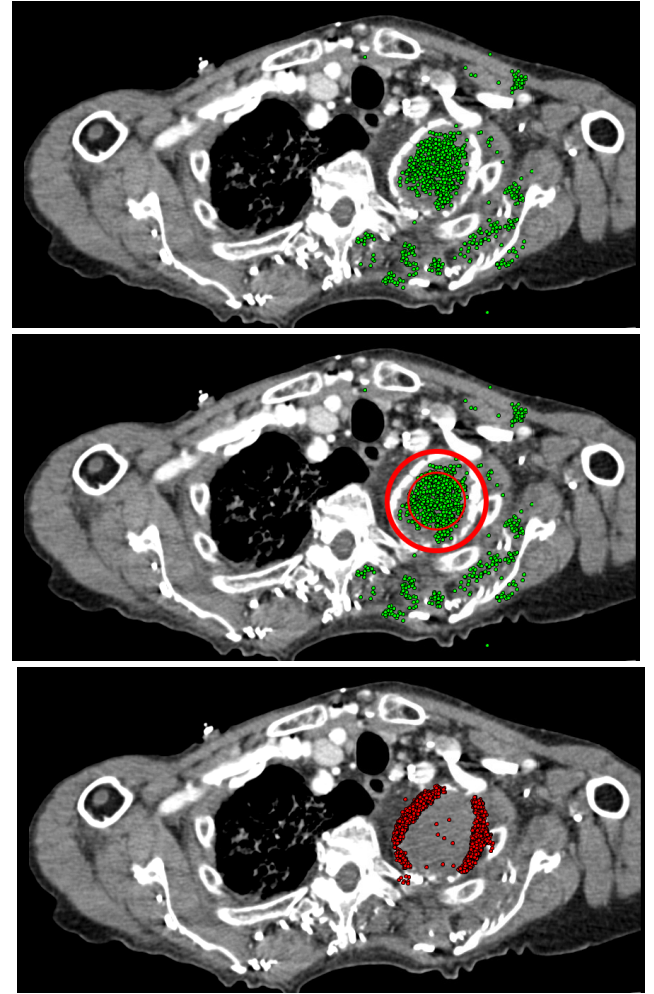


Fig. 11. Top: identifying the location of the diseased aorta within the scan; Middle: highlighting areas where potential calcifications might exist; Bottom: identification of calcification on the current slide of CT scan in order to compare with the others

comparing different parts of the aorta to choose the best possible location with the least level of calcium in the wall of the proximal neck to position the EVAR graft.

This can help assess CT angiography images of patients awaiting the repair of the aortic aneurysm. The SDS can evaluate all the CT slides that did look at the proximal neck to identify an optimal location for deploying the graft. This can reduce the risk of the proximal type I endoleak. This type of endoleak is the most serious complication of EVAR and it is a life threatening problem. When this occur the aneurysm sac is not excluded from the circulation and it can get larger and rupture causing a vascular catastrophe with 50-75% mortality rate.

D. Nasogastric Tube

In this experiment the SDS agents are applied to identify the tip of the NG tube that is the most radiopaque part. This can help clinicians identify the distal end of the tube and assess its position to ensure that it is in the stomach and not in the lungs (see Fig. 12).

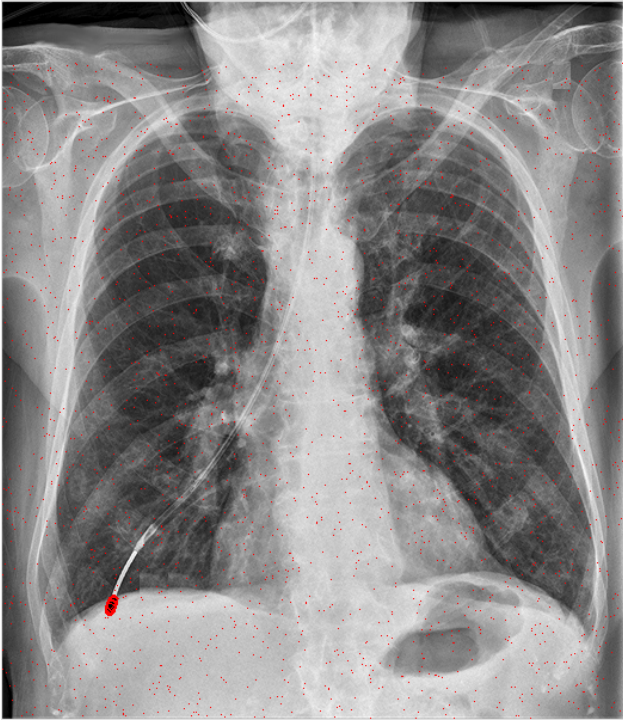


Fig. 12. Chest X-ray showing a misplaced Nasogastric tube detected by SDS

The adjustable parameters for this experiment are:

- $S = 10,000$
- $\alpha = 240$
- $\beta = 250$
- $dRad = 2$
- $Itr = 10$

The last three sections argue for the generalisation of the swarm intelligence technique presented in this paper. While the authors strongly keep themselves away from the any claim that the presented technique could replace human experts, the sample applications of this technique, shows the usefulness of the method and its possible potential to reduce human error and assist the identification of metastasis and micro-calcifications in various types of scans.

V. MAGNETIC RESONANCE (MR) BRAIN IMAGE SEGMENTATION USING HYBRID PSO-LVQ APPROACH

Learning Vector Quantisation (LVQ) is one of the primarily preferred Artificial Neural Network (ANN) for medical imaging applications. However, there are some hidden drawbacks associated with conventional LVQ which often go unnoticed. One of the significant drawbacks is the lack of convergence condition which forces the LVQ to completely depend on iterations. Any iteration dependent ANN becomes less accurate since correct fixation of the number of iterations is extremely difficult. If the number of iterations is not optimal, then the LVQ may encounter local minima problems. In this work, this specific problem is tackled by proposing a hybrid swarm intelligence-LVQ approach in the context of MR brain image

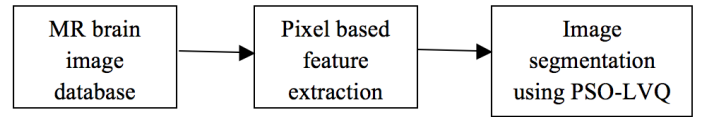


Fig. 13. Block diagram

segmentation. The Particle Swarm Optimization (PSO) is used to train the LVQ which eliminates the iteration-dependent nature of LVQ [19]. The proposed methodology is used to detect the tumour regions in the abnormal MR brain images.

A. Proposed Methodology

The framework of the proposed work is shown in Figure 13.

In this work, MR brain images collected from M/s. Devakai Scan Centre, Madurai, India is used for the experiments. Initially, six textural features are extracted from each pixel of the input image. The features used are mean, standard deviation, energy, entropy, variance and correlation. These features are estimated using a 33 window methodology. These features are further given as input for the PSO-LVQ for segmentation. The number of clusters used in this work is 4 which correspond to the Grey Matter (GM), White Matter (WM), Cerebro-spinal fluid (CSF) and the abnormal tumor region. The tumor portion is the region of interest in this work.

B. Architecture of PSO-LVQ

The architecture of PSO-LVQ consists of three layers: (a) the input layer, (b) the competitive layer and (c) the output layer. The framework is shown in Figure 14. The number of neurons in the input layer is six which is equal to the features extracted from each pixel. The number of output layer neurons is 4 which are equal to the number of pre-defined clusters. The competitive layer corresponds to the sub-classes and hence the number of neurons in this layer must be a multiple of the pre-defined classes. The number of neurons used in this work is 8 (two neurons for each class). Hence, the architecture of LVQ used is 6-8-4.

In figure 14, T corresponds to the correct category or class of the training input. The proposed architecture consists of a single weight matrix W whose values are determined during the training process. The neurons in the input layer are denoted by i and the neurons in the competitive layer is denoted by j .

C. Training algorithm of PSO-LVQ

PSO is a subset of swarm intelligence which is normally used for optimization applications. It is a population based search algorithm where each individual is referred to as particle and represents a candidate solution. Each single candidate solution is assumed to be an individual bird of the flock, i.e, a particle in the search space. Each particle makes use of its individual memory and knowledge to find the best solution. All the particles are given its own fitness values, which are evaluated by fitness function and have velocities which direct the movement of the particles. The particles move through the problem space by following a current of optimum particles. The initial swarm is generally created in such a way that

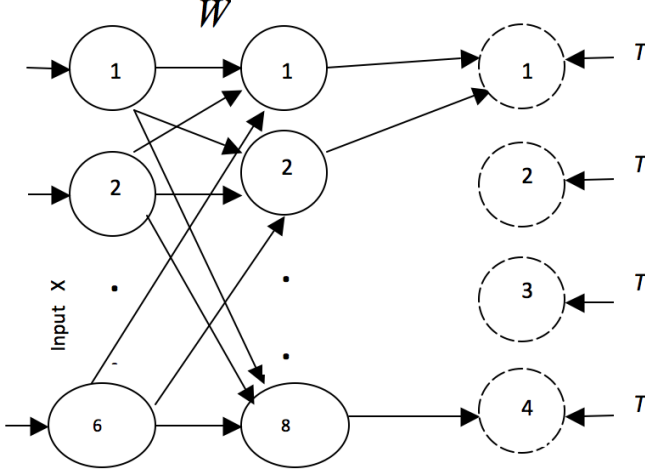


Fig. 14. Architecture of PSO-LVQ

the population of the particles is distributed randomly over the search space. At every iteration, each particle is updated by following two best values, called pbest and gbest. Each particle keeps track of its coordinates in the problem space, which are associated with the best solution (fitness value). This fitness value is called pbest. When a particle takes the whole population as its topological neighbor, the best value is a global best value and is called gbest.

In this work, a different dimension of PSO is explored in the context of training process of LVQ network. The main objective of the training process is to estimate the stabilized weights W . The proposed training algorithm of PSO-LVQ is given below.

Step 1: Supply the random weight matrix W , input x , c_1 and c_2 (cognitive and social acceleration factors, p (inertia factor), two random numbers (r_1, r_2) and initial velocity v_o .

Step 2: Calculate the Euclidean distance between the input vector and the weight matrix W

$$D_j = \|x_i - W_{ij}\| \quad (5)$$

Step 3: Find the neuron J such that $D(J)$ is a minimum. The weight values connected with this neuron are taken as the population for the PSO algorithm.

Step 4: Let the population of the PSO algorithm be taken as $w_t(m)$ where t is the iteration number and $m = 0, 1, 2 \dots s$.

Step 5: Find the fitness value for each member of the population using the fitness function. The fitness function used in this work is classification accuracy.

$$\text{If } f_t \geq f_{pbest} \text{ then } pbest(m) = w_t(m)$$

$$\text{If } f_t \geq f_{gbest} \text{ then } gbest = w_t(m)$$

Step 6: Update the particle velocity using the following equation:

TABLE II. DATASET USED FOR IMPLEMENTATION

Class	Training data (pixels/ image)	Testing data (pixels/image)
White matter	40	
Grey matter	40	65536 (Full image)
CSF	40	
Tumor	20	

$$v_{t+1}(m) = p \times (v_t(m)) + c_1 r_1 \times (pbest_t(m) - w_t(m)) + c_2 r_2 \times (gbest_t - w_t(m)) \quad (6)$$

Step 7: Update the weights using the following equations

If $T = C_j$, where C_j is a category or class represented by j^{th} unit, then

$$w_{t+1}(m) = w_t(m) + v_{t+1}(m) \quad (7)$$

If $T \neq C_j$, then

$$w_{t+1}(m) = |w_t(m) + v_{t+1}(m)| \quad (8)$$

Step 8: Increment m . If $m > s$, then increment t and set $m = 1$.

Step 9: Repeat steps 2 – 8 till the velocity reaches the minimum value. In this work, 0.01 is used as the minimum value. This implies that there will be no further changes in the weight values.

At the end of the training process, the stabilized set of weights W is stored and further used for the testing process. In the testing process, each pixel of the input image is classified into any one of the four clusters using these stabilized weights. The testing process is done with the conventional procedure of LVQ.

D. Experimental Results and Discussions

The software used for the implementation is MATLAB. The dataset used for the implementation is shown in Table II².

The table shows the training data and testing data for a single image. The same level of training data and testing data is used for all the images. The textural features extracted from the training data are shown in Table III.

The feature values shown in Table 2 are sufficiently unique for each category which aid in the successful segmentation by the proposed approach. The qualitative analysis of the PSO-LVQ based tumor detection in MR brain images is shown in Figure 15.

The experiments are conducted on 18 images but only samples are shown in Figure 15. Figure 15(a), (b) and (c) are the input images in which the abnormal tumor portion

²The training data are randomly selected.

TABLE III. FEATURE EXTRACTION RESULTS

Features	White Matter	Gray Matter	Cerebro-spinal fluid	Tumor
Energy	27891	256238	71236	124768
Correlation	-571	-1107	-74	-1.62E+003
Variance	1.24E+006	2.56E+007	6.20E+006	1.34E+007
Entropy	1.56E+003	7.83E+003	3.79E+003	5.68E+003
Mean	324571	154218	478642	567345
Standard deviation	1.55E+009	6.56E+011	3.84E+010	1.80E+011

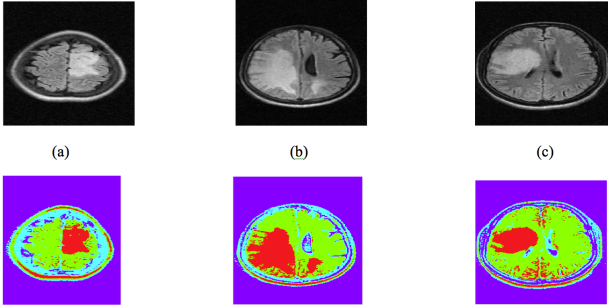


Fig. 15. Sample results: (a), (b), (c)- input images, (d), (e), (f) corresponding output images [red colour-tumor region, blue-white matter, violet-grey matter and yellow-cerebro spinal fluid]

is seen in white colour. In the segmented output, the red colour denotes the segmented tumor regions. A visual analysis reveals that PSO-LVQ has successfully segmented the tumor portion from the abnormal input image. However, the red colour portion seen in the outer ring actually corresponds to the skull tissues which act like abnormal tumor tissues. These unwanted skull tissues can be removed in the image pre-processing step to achieve better efficiency. A quantitative analysis on the segmented output images has been done in terms of *segmentation efficiency* which is the ratio of true positive pixels to the ground truth pixels. The quantitative analysis on the proposed approach is also performed which is shown in Table IV.

Sample results of the segmentation process are shown in Table 3. The same process is repeated for all the images and the average values are observed. An average segmentation efficiency of 88.5% has been achieved with the proposed PSO-LVQ approach. A comparative analysis of the proposed approach with the state-of-the art methods is shown in Table V.

From Table V, it is evident that the proposed method is efficient than other approaches in terms of performance measures.

VI. CONCLUSION

This paper details the promising results of the novel application of Stochastic Diffusion Search in detecting areas of metastasis in bone scans and the identification of the potential microcalcifications on the mammographs. Statistical and mathematical models are proposed to further investigate

TABLE IV. SEGMENTATION EFFICIENCY CALCULATION OF THE PROPOSED APPROACH

Input	Ground Truth	True positive	Segmentation
		pixels	efficiency (%)
Image 1	WM	11453	92.2
	GM	10936	82.3
	CSF	7128	90.2
	Tumor	5234	87.9
Image 2	WM	11453	90.6
	GM	10936	85.3
	CSF	7128	93.1
	Tumor	8178	93.4
Image 3	WM	11453	94.4
	GM	10936	84.1
	CSF	7128	94.2
	Tumor	6124	85.1

TABLE V. COMPARATIVE ANALYSIS

Techniques/Authors	Segmentation efficiency (%)
Self Organizing Map/Inan et.al. [20]	86
LVQ/Jinn-Yi et.al. [21]	86
Self Organizing Map/Merinsky et.al. [22]	70
K-means clustering/Javeed et.al. [23]	85
Fuzzy ANN/ Javeed et.al. [23]	84
Proposed Method (PSO-LVQ)	88.5

the behaviour of the agents in the population and the outcome demonstrates that the algorithm exhibits a statistically significant difference when applied to scans of variously affected individuals.

The swarms intelligence technique was also used in the two-phase process of the identification of aorta in the CT images, as well as calcifications in areas around the aorta; this task could lead to a more accurate localisation of the neck of the aneurysm.

Additionally, the swarms exhibited promising performance in detecting the tip of Nasogastric tube inserted through the nose to the stomach with the goal of providing short-term nutrition in critically ill patients. The identification of the tip of the tube by the swarms can in practice lead to reducing the probability of the complications of nasogastric tubes frequently caused by inadvertent malpositioning of the tube in the lungs versus stomach.

Furthermore, this work highlights the application of swarm intelligence techniques for MR brain segmentation. This work also portrays the advantages of swarm intelligence approaches in a different dimension. As a future work, the proposed approach will be compared with modified approaches such as adaptive chaotic PSO and hybrid kernel support vector machine.

At last not least, the authors would like to emphasise that the presented technique could be effectively utilised as an

adjunct to the expert's eyes of a specialist.

REFERENCES

- [1] J. Bishop, "Stochastic searching networks," in *Proc. 1st IEE Conf. on Artificial Neural Networks*, London, UK, 1989, pp. 329–331.
- [2] M. M. al-Rifaie and M. Bishop, "Stochastic diffusion search review," in *Paladyn, Journal of Behavioral Robotics*. Paladyn, Journal of Behavioral Robotics, 2013, vol. 4(3), pp. 155–173. [Online]. Available: <http://dx.doi.org/10.2478/pjbr-2013-0021>
- [3] M. M. al Rifaie, A. Aber, R. Sayers, E. Choke, and M. Bown, "Deploying swarm intelligence in medical imaging," in *Bioinformatics and Biomedicine (BIBM), 2014 IEEE International Conference on*. IEEE, 2014, pp. 14–21.
- [4] M. M. al-Rifaie, A. Aber, and R. Raisys, "Swarming robots and possible medical applications," in *International Society for the Electronic Arts (ISEA 2011)*, Istanbul, Turkey, 2011.
- [5] M. M. al-Rifaie, A. Aber, and M. Bishop, "Swarms search for cancerous lesions: Artificial intelligence use for accurate identification of bone metastasis on bone scans," *The European Federation of National Associations of Orthopaedics and Traumatology (EFORT), 13th EFORT Congress, Berlin, Germany*, 2012.
- [6] M. M. al-Rifaie and A. Aber, "Identifying metastasis in bone scans with stochastic diffusion search," in *Information Technology in Medicine and Education (ITME)*. IEEE, 2012. [Online]. Available: <http://dx.doi.org/10.1109/ITIME.2012.6291355>
- [7] M. M. al-Rifaie, A. Aber, and A. M. Oudah, "Utilising stochastic diffusion search to identify metastasis in bone scans and microcalcifications on mammographs," in *Bioinformatics and Biomedicine (BIBM 2012), Multiscale Biomedical Imaging Analysis (MBIA2012)*. IEEE, 2012, pp. 280–287. [Online]. Available: <http://dx.doi.org/10.1109/BIBM.2012.6470317>
- [8] K. Johnston, R. Rutherford, M. Tilson, D. Shah, L. Hollier, and J. Stanley, "Suggested standards for reporting on arterial aneurysms," *Journal of vascular surgery*, vol. 13, no. 3, pp. 452–458, 1991.
- [9] N. C. for Health Statistics, "Deaths, percent of total deaths and death rates for the 15 leading causes of death: United states and each state, 2000," *National Center for Health Statistics*, 2001.
- [10] K. Cassar, D. Godden, and J. Duncan, "Community mortality after ruptured abdominal aortic aneurysm is unrelated to the distance from the surgical centre," *British journal of surgery*, vol. 88, no. 10, pp. 1341–1343, 2001.
- [11] L. Brown, J. Powell *et al.*, "Risk factors for aneurysm rupture in patients kept under ultrasound surveillance," *Annals of surgery*, vol. 230, no. 3, p. 289, 1999.
- [12] F. Arko, K. Filis, S. Seidel, J. Gonzalez, S. Lengle, R. Webb, J. Rhee, and C. Zarins, "How many patients with infrarenal aneurysms are candidates for endovascular repair? the northern california experience," *Journal Information*, vol. 11, no. 1, 2004.
- [13] M. Armerding, G. Rubin, C. Beaulieu, S. Slonim, E. Olcott, S. Samuels, M. Jorgensen, C. Semba, R. Jeffrey, and M. Dake, "Aortic aneurysmal disease: Assessment of stent-graft treatment versus conventional angiography1," *Radiology*, vol. 215, no. 1, pp. 138–146, 2000.
- [14] W. Sternbergh, G. Carter, J. York, M. Yoselevitz, and S. Money, "Aortic neck angulation predicts adverse outcome with endovascular abdominal aortic aneurysm repair," *Journal of vascular surgery*, vol. 35, no. 3, pp. 482–486, 2002.
- [15] M. Robbins, B. Kritpracha, H. Beebe, F. Criado, Y. Daoud, and A. Comerota, "Suprarenal endograft fixation avoids adverse outcomes associated with aortic neck angulation," *Annals of vascular surgery*, vol. 19, no. 2, pp. 172–177, 2005.
- [16] B. Stanley, J. Semmens, Q. Mai, M. Goodman, D. Hartley, C. Wilkinson, and M. Lawrence-Brown, "Evaluation of patient selection guidelines for endoluminal aaa repair with the zenith stent-graft: the australasian experience," *Journal Information*, vol. 8, no. 5, 2001.
- [17] N. Guidelines, "Reducing the harm caused by misplaced nasogastric feeding tubes in adults, children and infants," *NHS*, 2011.
- [18] R. Miller, "Simultaneous statistical inference," *SPRINGER-VERLAG INC., 175 FIFTH AVE., NEW YORK, NY, 1981, 300*, 1981.
- [19] Y. Zhang, S. Wang, P. Phillips, and G. Ji, "Binary PSO with mutation operator for feature selection using decision tree applied to spam detection," *Knowledge-Based Systems*, vol. 64, no. 0, pp. 22 – 31, 2014.
- [20] İ. Güler, A. Demirhan, and R. Karakiş, "Interpretation of mr images using self-organizing maps and knowledge-based expert systems," *Digital Signal Processing*, vol. 19, no. 4, pp. 668–677, 2009.
- [21] J.-Y. Yeh and J. Fu, "A hierarchical genetic algorithm for segmentation of multi-spectral human-brain mri," *Expert Systems with Applications*, vol. 34, no. 2, pp. 1285–1295, 2008.
- [22] Z. Merinský, E. Hošťálková, and A. Procházka, "Brain tumour diagnostic support based on medical image segmentation," *brain*, vol. 40, no. 60, p. 80, 2009.
- [23] S. J. Hussain, T. S. Savithri, and P. S. Devi, "Segmentation of tissues in brain mri images using dynamic neuro-fuzzy technique," *International Journal of Soft Computing and Engineering (IJSCE) ISSN*, pp. 2231–2307, 2012.